



*atomic and molecular collisions group*

# *Excitation and Charge Exchange Phenomena in Astronomical Objects: Measurement of Cross Sections and Lifetimes*

*Presentation at the Topical Workshop on EUV and X-Ray Emission from Comets, Planets, and Heliospheric Gases*

*Jan. 16-17, 2003*

*A. Chutjian<sup>1</sup>, S. Smith<sup>1</sup>, J. Lozano<sup>1</sup>, I. Cadez<sup>2</sup>,*

*J. Greewood<sup>3</sup> R. Mawhorter<sup>4</sup>, I. Williams<sup>3</sup>, M. Niimura<sup>5</sup>*

*<sup>1</sup>Jet Propulsion Laboratory, Caltech, Pasadena, CA*

*<sup>2</sup>J. Stefan Institut, Ljubljna, Slovenia*

*<sup>3</sup>Queen's University, Belfast, UK*

*<sup>4</sup>Pomona College, Claremont, CA*

*<sup>5</sup>Plasma Physics Lab., UC California, Los Angeles, CA*

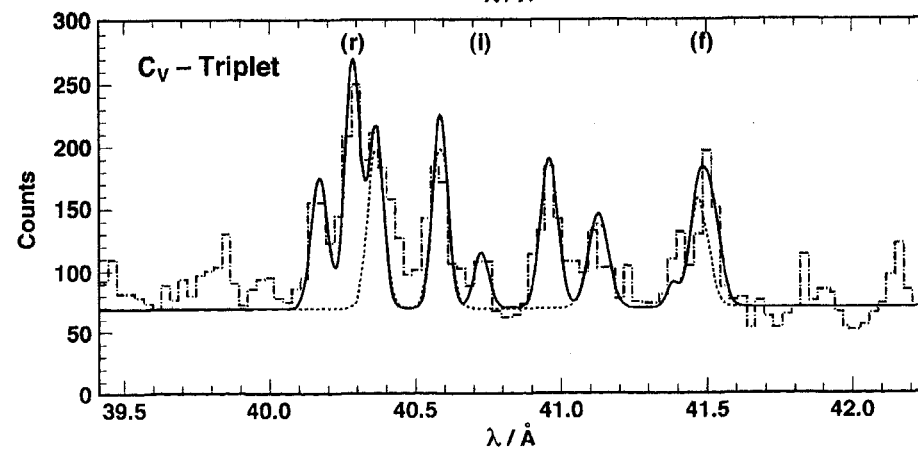
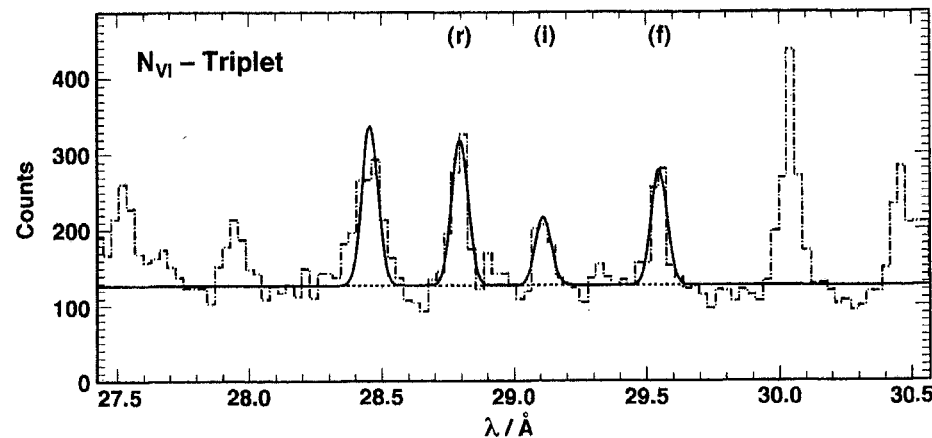
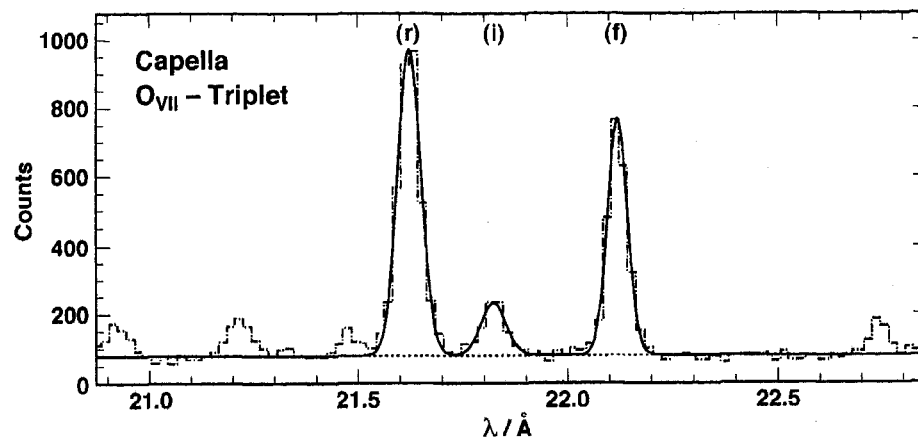
*The JPL work is supported under contract with NASA, and is carried out at JPL/Caltech.*

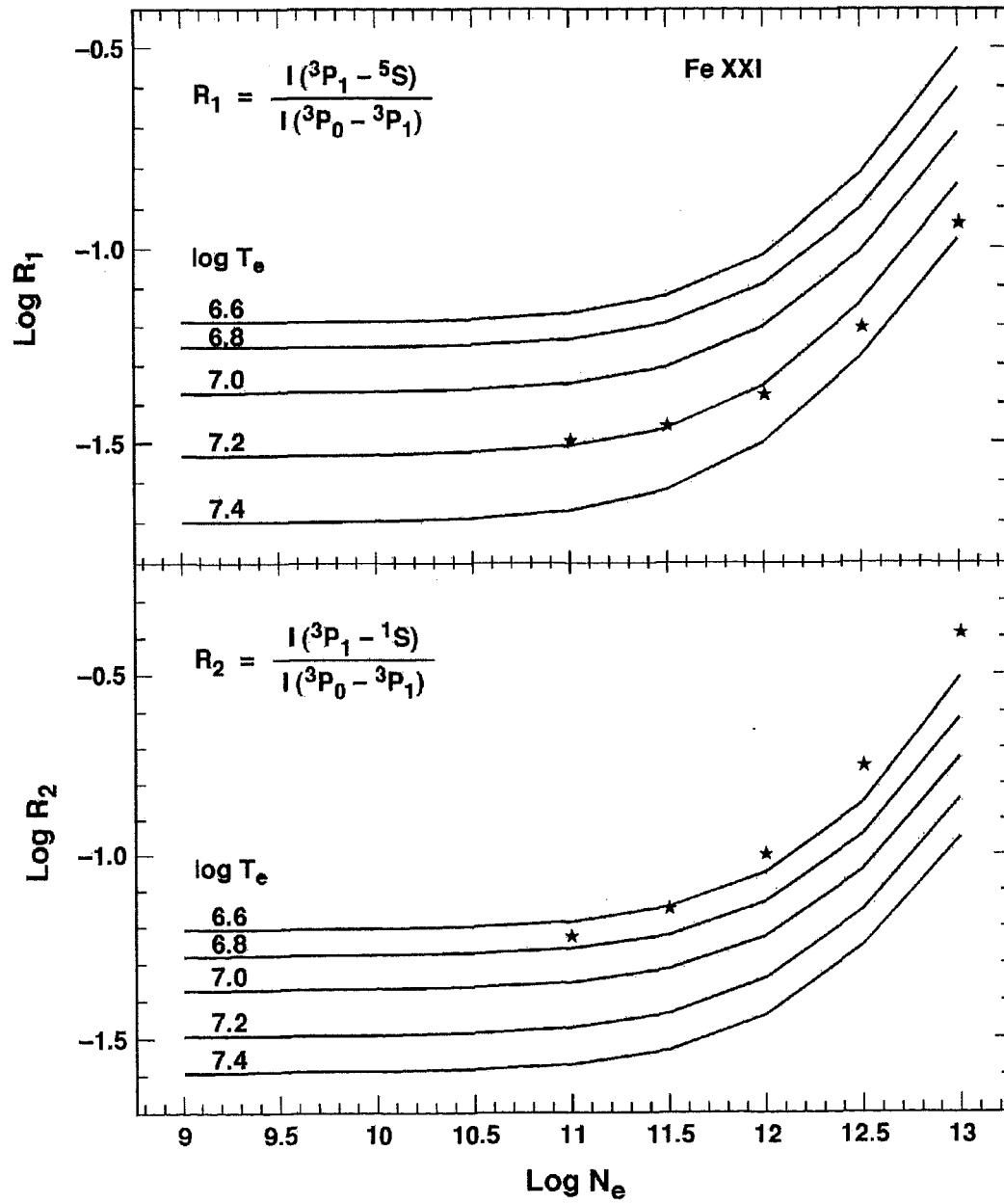
*CHANDRA/LETGS at Capella*

*r*:  $1s^2\ ^1S \rightarrow 1s2p\ ^1P^o$

*i*:  $1s^2\ ^1S \rightarrow 1s2s\ ^1S$

*f*:  $1s^2\ ^1S \rightarrow 1s2p\ ^3S$





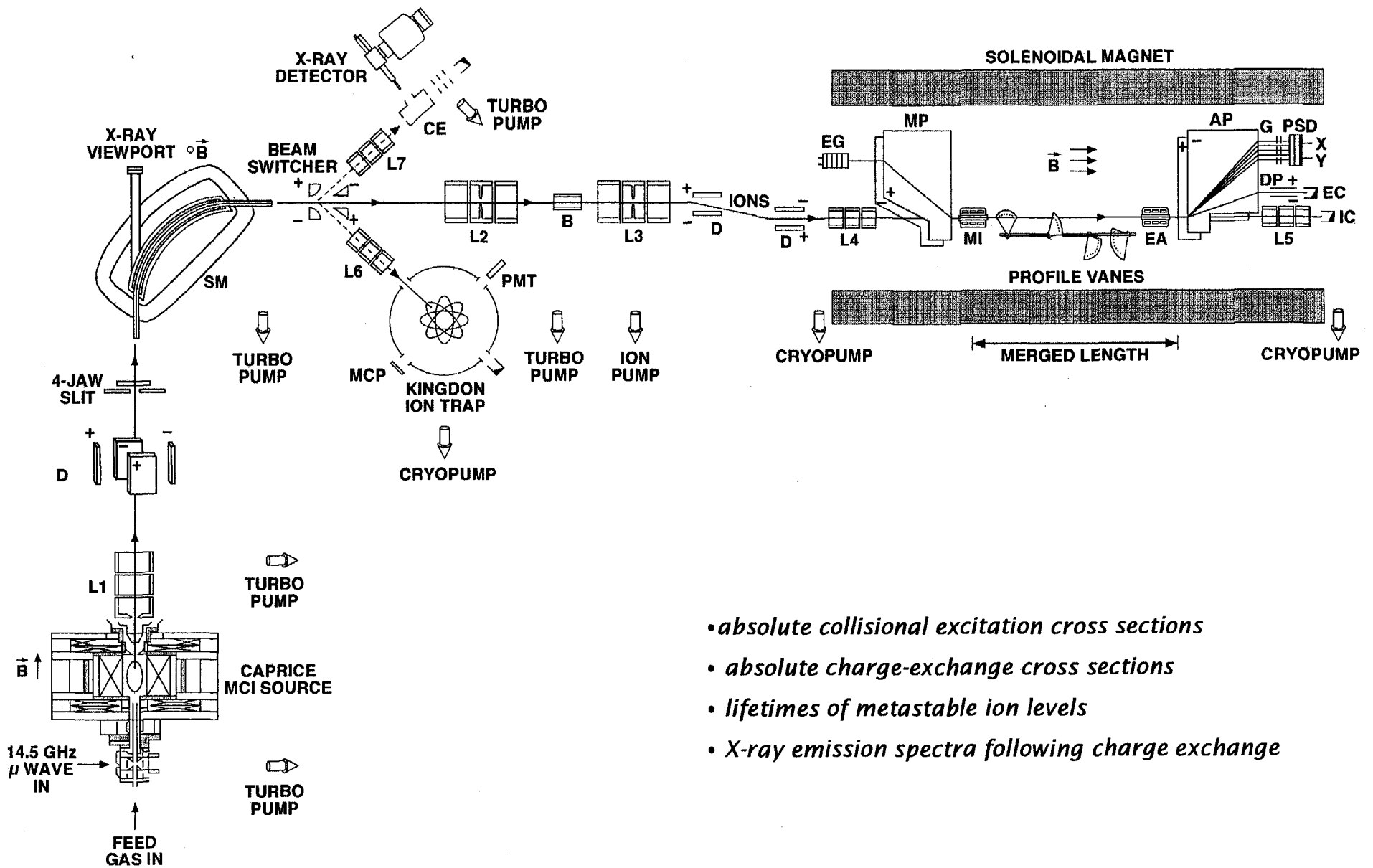
\* = DW calculation (Mason et al 1979)

— = 15-state R-Matrix (Keenan et al, 1996)

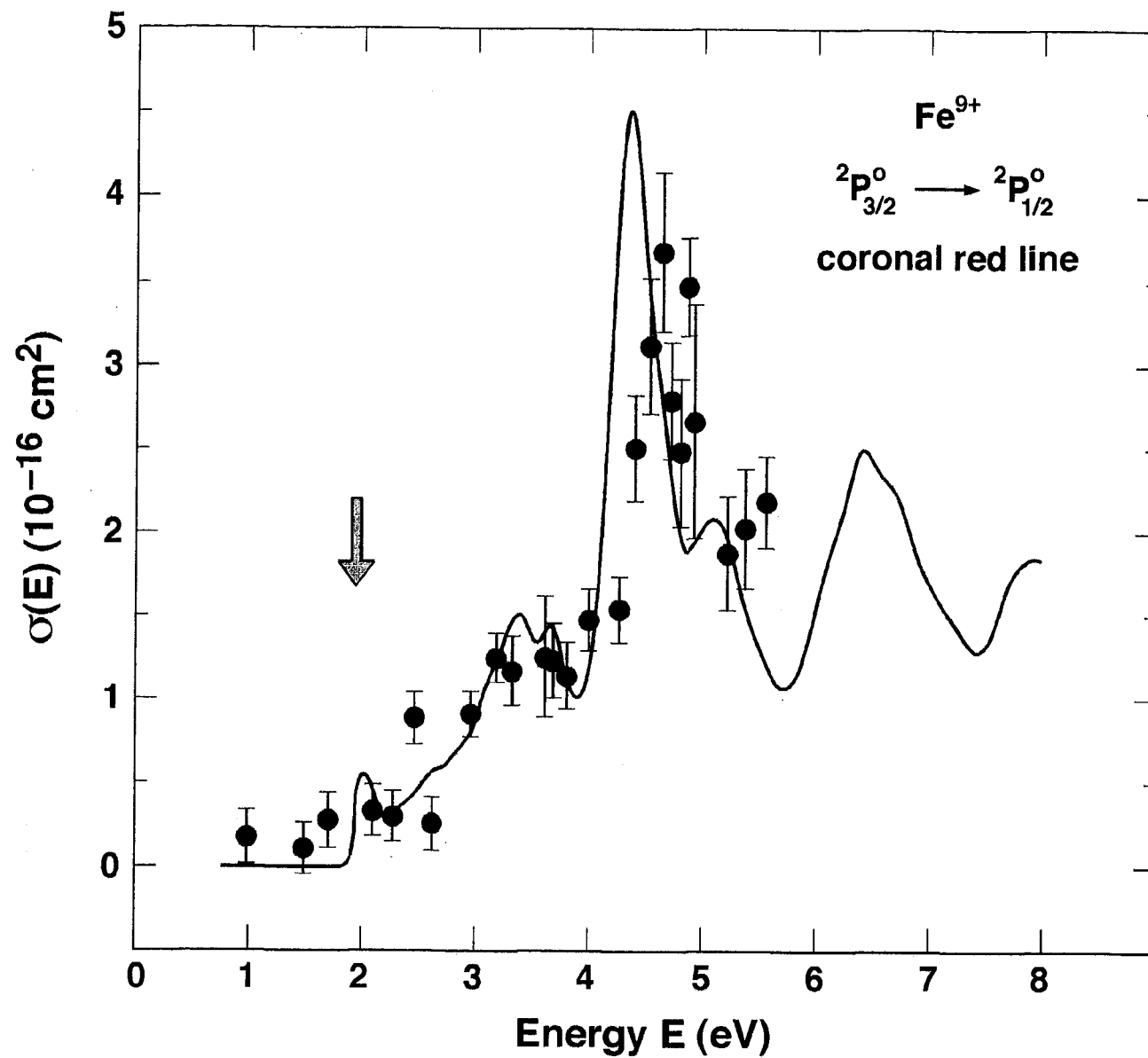
*Highly-charged heavy ions present in the solar wind, and their abundance relative to the total oxygen-ion abundance (taken as unity) (adapted from Schwadron & Cravens, 2000).*

HCl, X <sup>q+</sup>	[X <sup>q+</sup> ]/[O] fast	[X <sup>q+</sup> ]/[O] slow	Energy (keV)	
			fast	slow
C <sup>6+</sup>	0.085	0.318	35.0	9.95
C <sup>5+</sup>	0.440	0.210		
N <sup>7+</sup>	0.000	0.006	40.8	11.6
N <sup>6+</sup>	0.011	0.058		
N <sup>5+</sup>	0.127	0.065		
O <sup>8+</sup>	0.000	0.070	46.6	13.3
O <sup>7+</sup>	0.030	0.200		
O <sup>6+</sup>	0.970	0.730		
Ne <sup>8+</sup>	0.102	0.084	58.3	16.6
Ne <sup>7+</sup>	0.005	0.004		
Mg <sup>10+</sup>	0.029	0.098	70.0	19.9
Mg <sup>9+</sup>	0.044	0.052		
Mg <sup>8+</sup>	0.028	0.041		
Mg <sup>7+</sup>	0.007	0.017		
Mg <sup>6+</sup>	0.003	0.009		
Si <sup>10+</sup>	0.024	0.021	81.6	23.2
Si <sup>9+</sup>	0.045	0.049		
Si <sup>8+</sup>	0.022	0.057		
Si <sup>7+</sup>	0.002	0.000		
S <sup>11+</sup>	0.001	0.000	93.3	26.5
S <sup>10+</sup>	0.008	0.005		
S <sup>9+</sup>	0.027	0.016		
S <sup>8+</sup>	0.023	0.019		
S <sup>7+</sup>	0.005	0.006		
S <sup>6+</sup>	0.001	0.002		
Fe <sup>13+</sup>	0.005	0.002	163	46.4
Fe <sup>12+</sup>	0.017	0.007		
Fe <sup>11+</sup>	0.025	0.023		
Fe <sup>10+</sup>	0.025	0.031		
Fe <sup>9+</sup>	0.015	0.041		
Fe <sup>8+</sup>	0.005	0.034		
Fe <sup>7+</sup>	0.001	0.007		

# Plan of the JPL Highly-Charged Ion Facility



- absolute collisional excitation cross sections
- absolute charge-exchange cross sections
- lifetimes of metastable ion levels
- X-ray emission spectra following charge exchange



- *absolute excitation measurements (JPL, Niimura et al 2002)*
- *49-state Breit-Pauli calculations*

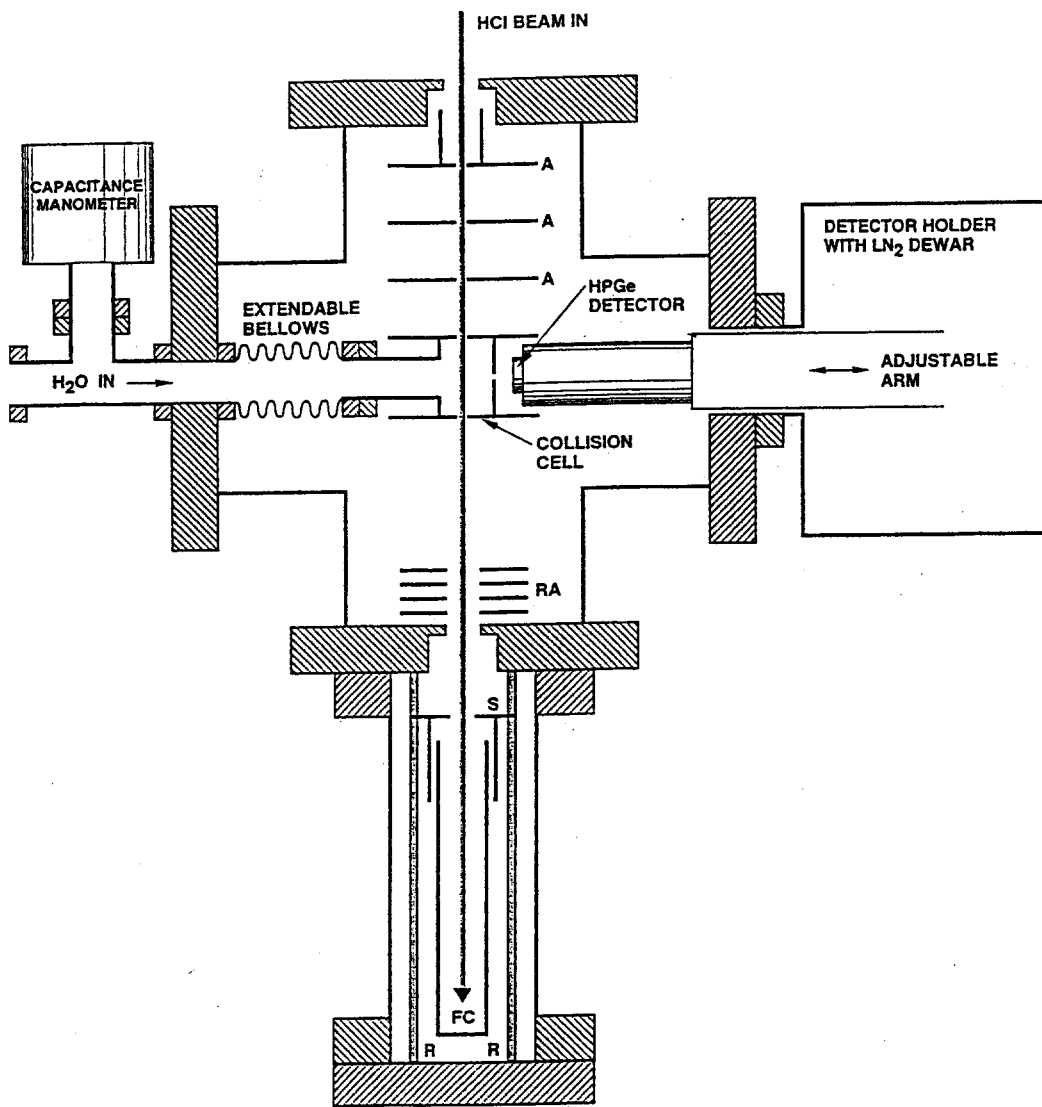


FIG. 1. Details of the charge-exchange beamline. The definitions are A, input HCI beam-defining apertures; RA, retarding-field apertures; S, secondary-electron shield; FC, Faraday cup; R, support rods; LN<sub>2</sub>, liquid nitrogen.

$$V_R = \frac{qV_0}{(q-j)}, \quad (2)$$

where  $V_0$  is the source voltage. Thus, it is possible to reflect the primary ion beam while charge-exchanged ions are transmitted. By raising this reflecting potential, ion currents from single and multiple charge exchanges are measured. This electric field is produced by a series of four apertures, the center two are held at the required reflecting potential, the end two at ground potential. The apertures have a large diameter and are widely spaced to give field lines that are almost parallel near the beam axis. They are also placed close to the Faraday cup to ensure that all transmitted ions are collected.

The pressure of gas in the cell is held low so that only about 1% of the ion beam charge exchanges, ensuring single-collision conditions. The cross section for the charge exchange is determined from the relationship

$$\sigma_{q,q-j} = \frac{kT}{PL} \frac{qI_{q-j}}{(q-j)I_q}, \quad (3)$$

where  $L$  is the collision length,  $T$  the gas temperature,  $I$  and

currents  $I_{q-j}$  are measured in the same Faraday cup using the same electrometer and scale. Hence any systematic error in the absolute current measurement is eliminated in the above formula. This is an advantage over the use of channel-type multipliers, for which a linear response to ion current must be assumed. Electrometer and capacitance manometer zero offset and drift are taken into account when making measurements.

Errors in the measurements mainly arise from the pressure measurement and instability of the ion beam. As  $I_{q-j}$  and  $I_q$  cannot be measured simultaneously, a drift in ion beam current is unwelcome. In practice  $I_{q-j}$  and  $I_q$  are measured alternately multiple times, and the measurements of  $\sigma_{q,q-j}$  are averaged. The standard deviation of these results is used to determine the random error due to the variability of the ion beam.

A 2-mm aperture in the cell wall allows x-rays to escape. A high-purity Ge solid state EG&G IGLET-X detector [43] with a high detection efficiency and moderate resolution is located at right angles to the beam axis. A 7.5- $\mu\text{m}$ -thick Be window isolating the detector from the vacuum chamber introduces a transmission factor dependent on the energy of the x-rays. The detector can be translated inside a flexible hel

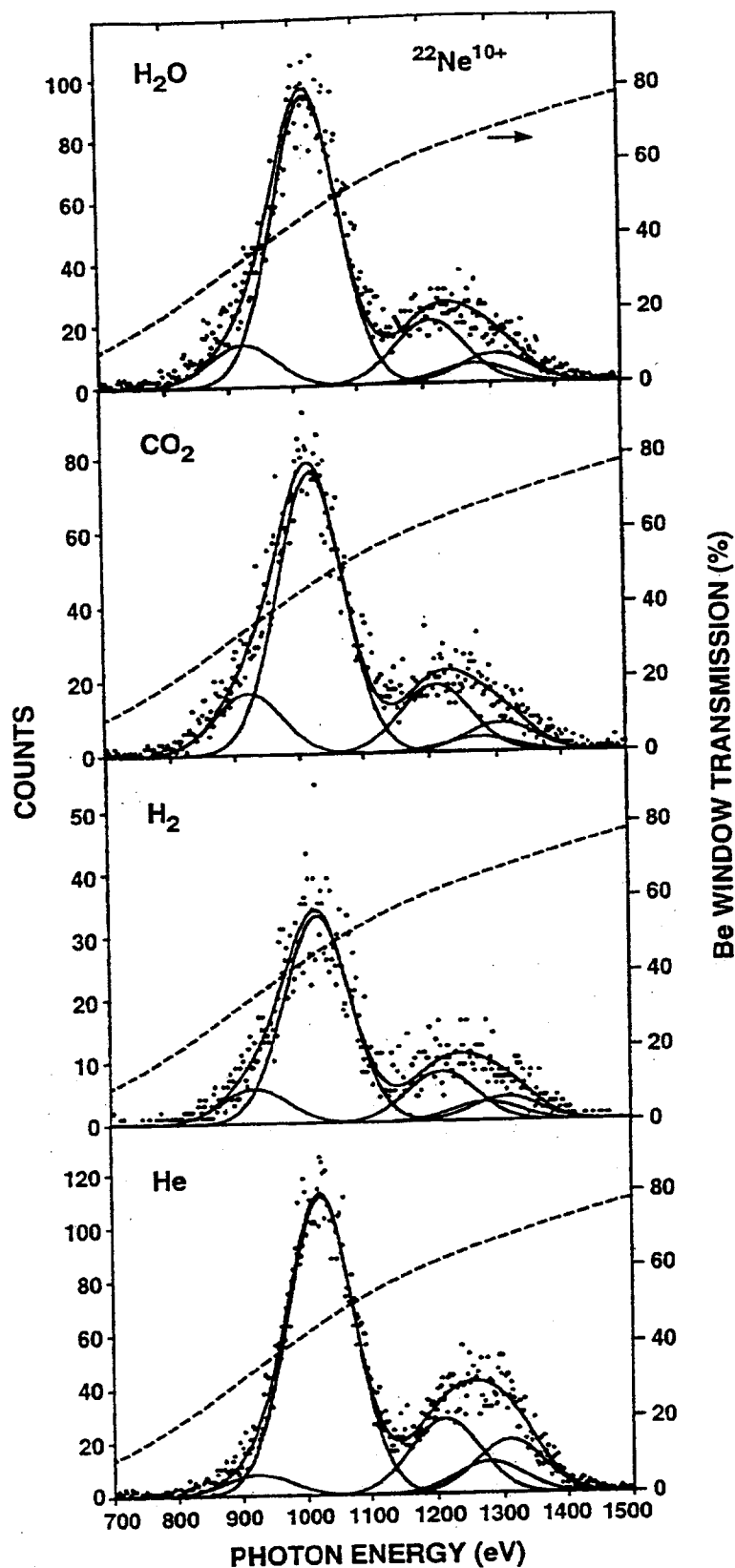


FIG. 4. X-ray spectra from collisions of  $\text{Ne}^{10+}$  in He,  $\text{H}_2$ ,  $\text{CO}_2$ , and  $\text{H}_2\text{O}$ , uncorrected for transmission of the Be window on the Ge x-ray detector (given as a dashed line). The underlying curves are the Ly transitions  $np \rightarrow 1s$ .

have  $P=0.6$ . Given the expected that alignment for these transitions.

The relative contributions determined from the area divided by the transmission, normalizing the total spectrum to the total cross section with line-emission contributions are shown in Tables I and II.

The x-ray spectrum consists of contributions from cascading transitions from  $p$  orbitals. The proportion of these contributions to the  $2s$  metastable level is determined by the branching ratios determined from a statistical model. If a statistical fraction is less than 0.5, the relative contribution is less than 0.5.

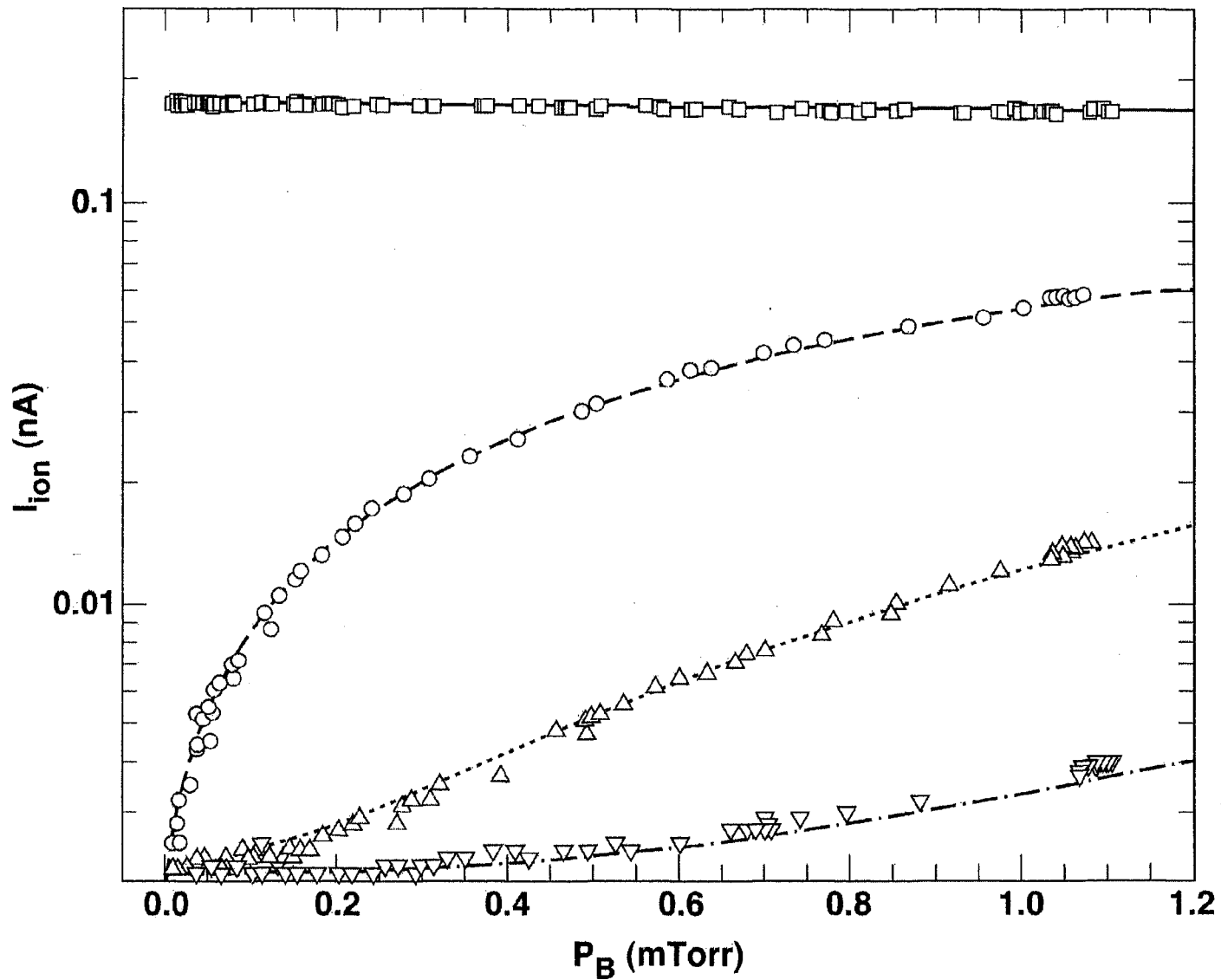
Double capture can lead to He-like Ly $\alpha$  which preferentially enhances the Ly $\alpha$  transition [29], enhancing the Ly $\alpha$  transition from Figs. 4 and 5. Its intensity is lower at lower ionization potentials. The value of the initial  $n$  is determined by the capture process.

With the scheme described here, we can obtain information about the initial capture process. Theoretical predictions including a statistical model for the contributions from the Ly $\alpha$  transition. From this analysis the Ly $\alpha$  transition is used to obtain a value for the initial  $n$ . It should be noted that the contributions from a Ly $\alpha$  transition to enhance the Ly $\alpha$  transition can be regarded as upper limits.

The results show that the Ly $\alpha$  transition is consistently lower than the Ly $\alpha$  transition. This is not surprising because the Ly $\alpha$  transition would not have a capture velocity of 0.3. The Ly $\alpha$  transition is  $l=n-1$ . The values of the Ly $\alpha$  transition are shown in Tables I and II.

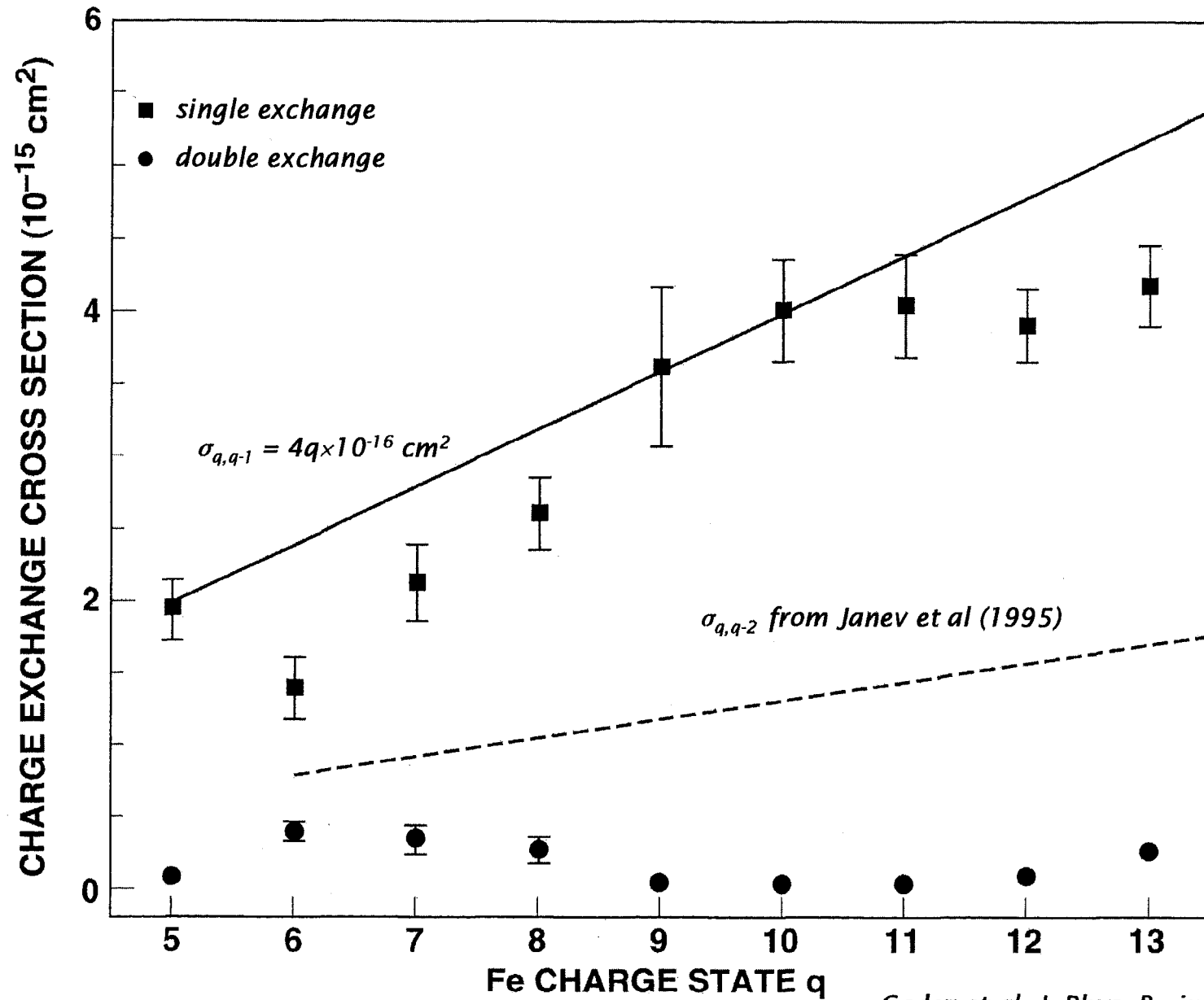
$$I_0(1 - P \cos^2 \theta) \quad (6)$$





*Ion-Current Variation with target gas pressure for 84 keV  $^{56}\text{Fe}^{12+}$  in He*

- |           |                       |             |                       |
|-----------|-----------------------|-------------|-----------------------|
| $\square$ | $V_{retard} = 6.0$ kV | $\triangle$ | $V_{retard} = 8.0$ kV |
| $\circ$   | $V_{retard} = 7.4$ kV | $\nabla$    | $V_{retard} = 8.8$ kV |



*Cadez et al, J. Phys. B., in preparation*

Radiative lifetimes  
( $\tau = 541$  ms) in the  
M1 transition  $2s^2 2p^2$   
 $^1S_0 \rightarrow ^3P_1$  at 232.17  
nm (Smith et al, PRA,  
to be submitted).

